Int. J. Electrochem. Sci., 15 **(2020)** 5395 – 5403, doi: 10.20964/2020.06.31

International Journal of
ELECTROCHEMICAL
SCIENCE
www.electrochemsci.org

Short Communication

Using Voltammetry and EIS for Analysis of Pottery Materials

Guangfu Liu[1,], Xinghua Yang[1], Huaiwei Zhang[2] and Li Fu[1,2*]*

[1] Henan Key Laboratory of Research for Central Plains Ancient Ceramics, Pingdingshan University, Pingdingshan Henan, 467000 PR. China
[2] College of Materials and Environmental Engineering, Hangzhou Dianzi University, Hangzhou 310018, PR. China
[*]E-mail: 415lgp@163.com; Li Fu fuli@hdu.edu.cn;

Received: 2 February 2020 / *Accepted:* 29 March 2020 / *Published:* 10 May 2020

Due to the different materials and/or different production conditions used to make pottery, including temperature, roasting time and oxidation/reduction conditions, the voltammetric signal of pottery powder could be used for potential archaeological analysis. In this work, we selected black pottery, gray pottery and red pottery as examples to confirm the hypothesis. Differential pulse voltammetry and electrochemical impedance spectroscopy were used as analytical methods. The results indicate that the voltammetric signals of Mn and Fe species in the pottery samples could be used as evidence for pottery identification. The observed difference was also confirmed by XRF analysis and physical property analysis.

Keywords: Voltammetric signal; Pottery analysis; Electrochemistry; Electrochemical impedance spectroscopy; Solid-state electrochemistry

1. INTRODUCTION

China has the longest history of ceramics in the world, but for a long time, this country has had a lack of complete historical records and systematic research. As an independent subject, the study of ancient ceramics began in the 1930s, integrating the fields of archaeology, materials science, computer science, physics and chemistry and belonging to a new interdisciplinary subject. The study of ancient ceramics does not use the traditional methods of observation and touch to verify authenticity but can determine the chemical components of ceramic samples and study them from a scientific viewpoint.

In 1869, M. Fouque used chemical methods to analyze the origin of ancient ceramics unearthed in pottery with holy origins. In 1928, Dr. F. G. Jackson and Prof. W. Bradfield analyzed ceramics and slurry by the wet chemical method. In 1954, Robert Oppenheimer, a famous American nuclear physicist, with E. V. Sayre and R. W. Dodson of the Department of Chemistry of Princeton University studied the

origin of ancient ceramics in the Mediterranean region by neutron activation analysis [1]. In 1969, Tite [2] determined the sintering temperature of a series of ceramics of different origins and ages by the thermal expansion method. Meloni S. et al. [3] studied the production process and origin of Roman Pavia pottery by neutron activation analysis. Maniatis et al. [4] observed a series of Neolithic pottery using SEM. Since then, many scholars have also studied the chemical composition, firing process and mineral composition of ancient pottery [5–7].

Composition analysis is one of the most popular methods in the study of ancient ceramics. Through the elemental analysis of ceramic samples, information on the raw material formula and production process can be obtained [8–10]. Elemental analysis can also be used for dating and origin analysis criteria. Commonly used methods in the study of ancient ceramics include X-ray fluorescence (XRF) [11–14], neutron activation analysis (NAA) [15–18], inductively coupled plasma mass spectrometry (ICP-MS) and inductively coupled plasma atomic emission spectrometry (ICP-AES) [19–23].

XRF is the main method used to analyze the primary and secondary elements of ancient ceramic samples. According to the different dispersion modes, XRF can be divided into two categories: wavelength-dispersive X-ray fluorescence (WD-XRF) and energy-dispersive X-ray fluorescence (ED-XRF). According to Bragg's law, WD-XRF uses spectroscopic crystals to separate the fluorescence signals of different wavelengths for measurement. Depending on the pulse height of the detector signal, ED-XRF is proportional to the energy of the X-ray photon and uses a multichannel analyzer to process fluorescence signals of different energies [24–27]. The WD-XRF detector is composed of a scintillation counter tube and a proportional counter tube. The counting rate is high, and it can use a strong X-ray excitation source, so the sensitivity is high. Due to the use of a variety of spectroscopic crystals, the resolution is higher than other methods, which is conducive to the analysis of light elements. Compared with ED-XRF, the mechanical part of the WD-XRF instrument is more complex, and the sample chamber of the WD-XRF instrument is small, so it is not suitable for the nondestructive analysis of complete ancient ceramic objects or large fragments.

The solid voltammetric method proposed by Scholz et al. [28,29] can be used to obtain information about the composition of materials used in ancient ceramics. This new method can be applied to insoluble solids, for example, by providing qualitative and quantitative information and structural information with a small amount of soluble solids [30–32]. The method requires only a nanogram-microgram sample. The first cultural relic analysis report based on solid-state electrochemical analysis technology was proposed in 1995 [33]. Irradiation defects formed by the long-term accumulation of natural radiation and cosmic rays in ceramic artifacts can be used as electrocatalytic centers for oxygen evolution reactions (OERs) [34–41]. The current intensity of the OER is positively correlated with the accumulated radiation amount in ceramic relics, so it can be used for the chronological analysis of ceramic relics. In approximately 2000, Domenech-Carbo's team started working on mineral pigments based on solid-state electrochemical analysis. Through the comparison between standard mineral pigments and variograms sampled from ancient ceramics, the identification and analysis of pigments in cave paintings, sculptures, church decorations and ancient oil paintings were successfully realized [42,43]. After 2002, Domenech-Carbo's team began to analyze trace metal oxides in ancient ceramic enamel using solid-state electrochemical analysis techniques [44–46]. In this work,

we specifically focused on the possibility of using the voltammetric method for pottery analysis. Three different pottery samples, including black pottery, gray pottery and red pottery, were chosen for analysis. Both voltammetric scanning and electrochemical impedance spectroscopy (EIS) were used. In addition, the XRF method has been used for elemental analysis as well as for explaining the difference observed from the electrochemical profiles.

2. MATERIALS AND METHODS

In this study, five individual gray pottery, black pottery and red pottery were applied for analysis. These potteries were purchased from local nursery without further treatment. Their elemental information has been supplied in Table 1. Pottery particles were collected by rasp the intersection of pottery tile. Then, the pottery particles were added into 1 mL of water followed with a 2 min sonication. Then, 5 μL of the dispersion was dip-coated on the glassy carbon electrode and dried in the room-temperature. All chemicals were analytical-grade reagents and were used without further purification. Milli-Q water (18.2 MΩ/cm) was used throughout the experiments.

The voltammetric signal of the pottery samples was recorded with a CHI660C workstation using a three-electrode system, and a 0.1 M H_2SO_4 aqueous solution was used as the electrolyte. Differential pulse voltammetry was used to record the electrochemical fingerprints of all plant tissues between -1 and 1.4 V with a pulse amplitude of 50 mV, a pulse width of 0.05 s and a pulse period of 0.5 s. EIS measurements were performed in a 0.1 M KCl solution including 1.0 mM $[Fe(CN)_6]^{3-/4-}$ with a frequency range from 10^4 to 0.1 Hz.

The physical properties of ceramics are analyzed as follows: Dried pottery shards are placed on an electronic scale to measure the dry weight, and then the sample is placed in an airtight container. After vacuuming to 8 Pa, water is released into the container through an outside pipe until the water covers the sample. After 15 min, the sample is removed from the container, and then the suspension weight and wet weight of the sample are measured. The water absorption, porosity, surface density and volume density of the sample can be obtained.

3. RESULTS AND DISCUSSION

Figure 1 shows a schematic diagram of the voltammetric signal recording of pottery powder by the electrochemical method. Chitosan was added to firmly fix the powder on the surface of the electrode. The voltammetric signal was recorded in 0.1 M H_2SO_4. These voltammetric signals represent the electrochemical reactions of oxidizable and reducible compounds in pottery powders. Because of the differences in firing temperature, raw material use, and preparation methods of different types of potteries, these signals can be used as fingerprints for potential archaeological analysis.

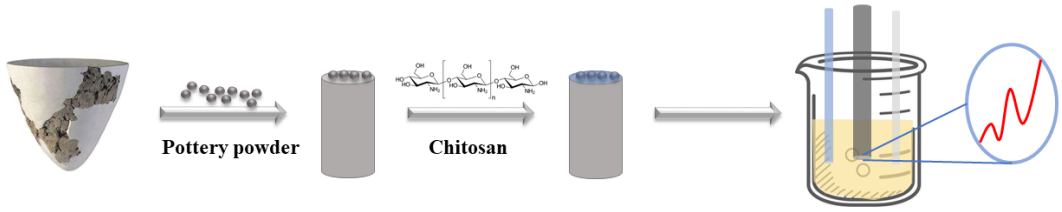

Figure 1. Schematic diagram of the recording voltammetric signal of pottery powder.

Figure 2 shows the anodic DPV scanning curves of black pottery, gray pottery and red pottery in 0.1 M H_2SO_4. As seen from the figure, there is only one obvious HER peak between -1.0 and 0 V. Between 0 and 1.0 V, we observe three distinct oxidation peaks. According to the literature [47–51], the two oxidation peaks at the lower potential are the oxidation of iron with a low oxidation state. The third peak near 1.0 V is an OER process caused by manganese catalysis [52]. At the same time, a significant oxidation peak above 1.0 V was caused by the OER on the electrode surface.

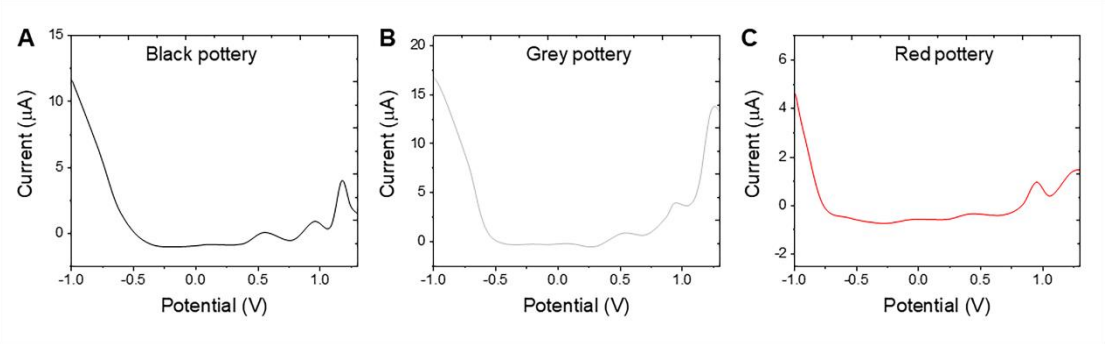

Figure 2. Anodic scan curves of (A) black pottery, (B) gray pottery and (C) red pottery in 0.1 M H_2SO_4.

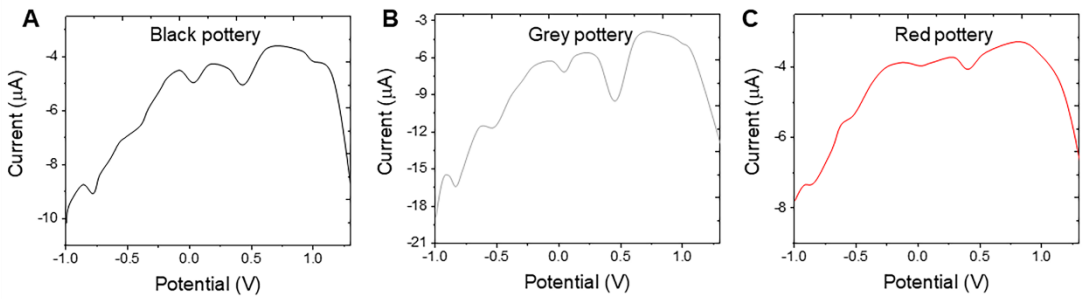

Figure 3. Cathodic scan curves of (A) black pottery, (B) gray pottery and (C) red pottery in 0.1 M H_2SO_4.

Figure 3 shows the cathodic DPV scanning curves of the black pottery, gray pottery and red pottery in 0.1 M H_2SO_4. It can be seen that a very weak reduction peak can be noticed at approximately 0.8 V, which is the reduction reaction of manganese dioxide [53]. Between 0.6 and -0.6 V, we can see three very obvious reduction peaks. These peaks are the reduction reactions of iron in different valence

states. In addition, there is a very obvious reduction peak at -0.7 V, which can be attributed to the ORR process.

As seen from Figure 1 and Figure 2, both the anode and cathode scanning results of the DPV of black pottery, gray pottery and red pottery have similar trends, but we can still observe differences in the peak position and peak shape. These differences are due to the different materials and/or different production conditions used to make the pottery, including temperature, roasting time and oxidation/reduction conditions [54]. Therefore, we performed repeated tests on different pottery samples. We chose five black pottery, gray pottery and red pottery samples. We repeated the test 5 times for each pottery sample and used the third iron oxidation peak and the first reduction peak of hematite as markers. Figure 4 shows the data plot of all the test results of black pottery, gray pottery and red pottery. As seen from the figure, the voltammetric signal ratio of the same sample is very similar, but there are some differences between different samples, which is a reasonable result. It is impossible to guarantee that the components in each product are exactly the same. At the same time, it is impossible to ensure that the heating environment of all products is the same during the firing process. In contrast, much larger differences can be detected among black pottery, gray pottery and red pottery. The voltammetric signal data correspond to the XRF data. Table 1 shows the XRF results for all pottery samples. As seen from the table, black pottery has the highest content of iron oxide among the three sample types. At the same time, gray pottery has the lowest content of manganese oxide, and one of the samples had no detectable content of manganese oxide. In contrast, the iron oxide and manganese oxide contents of the red pottery sample are between those of the black pottery and gray pottery.

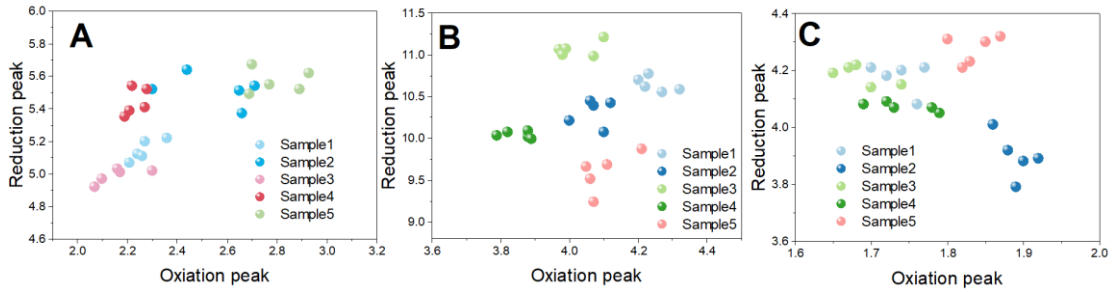

Figure 4. Plots of iron oxidation *vs.* hematite reduction from voltammograms for (A) black pottery, (B) gray pottery and (C) red pottery.

Table 1. XRF results and all pottery samples.

No.	Type	Na_2O	MgO	Al_2O_3	SiO_2	K_2O	CaO	TiO_2	MnO	Fe_2O_3
1	Black	1.41	1.08	18.24	64.52	3.21	0.88	0.41	0.10	10.15
2	Black	1.55	1.05	18.50	63.22	3.25	0.53	0.48	0.07	11.35
3	Black	1.67	1.06	19.51	63.41	3.55	1.06	0.39	0.08	9.27
4	Black	1.32	1.00	17.51	63.59	3.65	0.56	0.33	0.11	11.93
5	Black	1.66	0.57	19.25	61.47	3.12	0.69	0.41	0.10	12.73
1	Gray	0.09	1.32	22.07	65.52	2.98	1.12	0.08		6.82
2	Gray	0.14	1.27	24.06	66.68	2.58	1.52	0.09	0.07	3.59

3	Gray	0.18	1.20	24.08	65.24	2.88	1.06	0.35	0.05	4.96
4	Gray	0.16	1.55	23.51	63.59	3.02	1.65	0.21	0.06	6.25
5	Gray	0.17	1.36	22.51	64.51	2.68	1.52	0.84	0.07	6.34
1	Red	3.52	1.24	19.51	63.77	2.01	0.85	0.24	0.11	8.75
2	Red	3.17	1.20	20.51	62.09	2.09	0.86	0.65	0.10	9.33
3	Red	3.20	1.08	18.56	62.56	2.33	0.88	0.41	0.09	10.89
4	Red	3.65	1.21	16.87	63.58	2.08	0.87	0.55	0.12	11.07
5	Red	2.96	1.04	21.51	62.04	1.98	0.79	0.32	0.04	9.32

Figure 5 shows the water absorption, porosity, surface density and volume density of all pottery samples. It can be seen from the figure that the variation trends of the water absorption and porosity of the samples are basically the same. As seen from the graph of the water absorption rate and porosity, the water absorption rate and porosity of gray pottery are larger than those of black pottery and red pottery, indicating that the compactness of different pottery samples is quite different, and the firing process is different. As seen from the density comparison, the density of the three types of pottery is not very different.

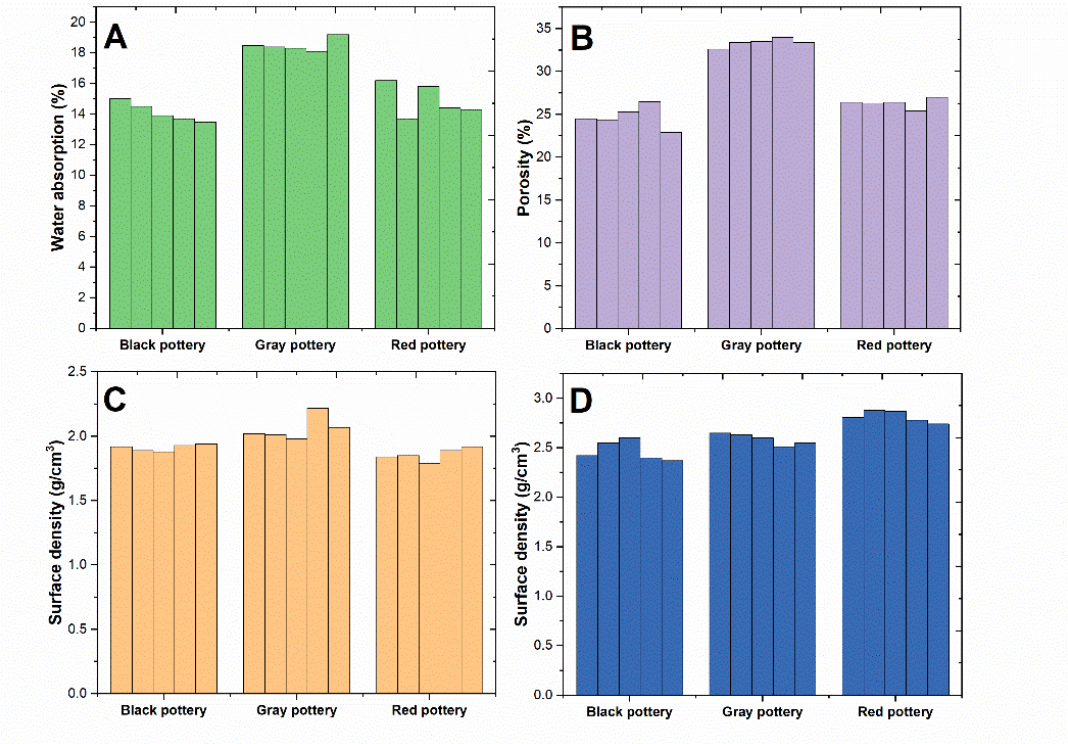

Figure 5. (A) Water absorption, (B) porosity, (C) surface density and (D) volume density of all pottery samples.

EIS of pottery powders was conducted using dissolved oxygen in the electrolyte as a probe. Figure 6A shows the Nyquist plots of black, gray, and red pottery. As seen from the figure, the EIS spectrum has only one significant capacitance loop. Figure 6B shows the corresponding Bode diagram.

We can see two relative responses in the total impedance and phase angle changing with frequency. The EIS data were then analyzed by the method proposed by La-Torre-Riveros et al. [54] using the logarithm of the total impedance at the low extreme of tested frequencies and the logarithm of frequency. In this way, different kinds of ceramics can be clearly distinguished (Figure 7).

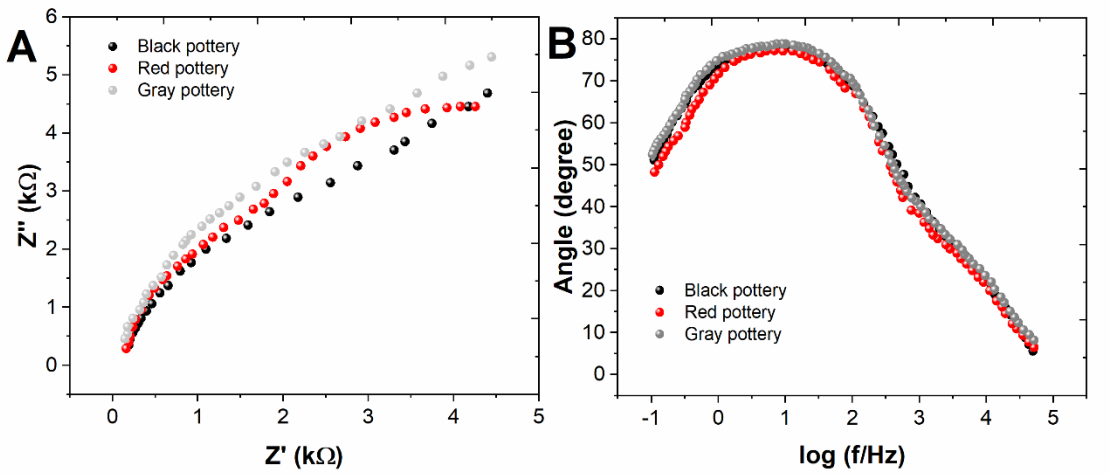

Figure 6. (A) Nyquist and (B) Bode plots of black pottery, gray pottery and red pottery in contact with air-saturated 0.10 M H_2SO_4 aqueous solution.

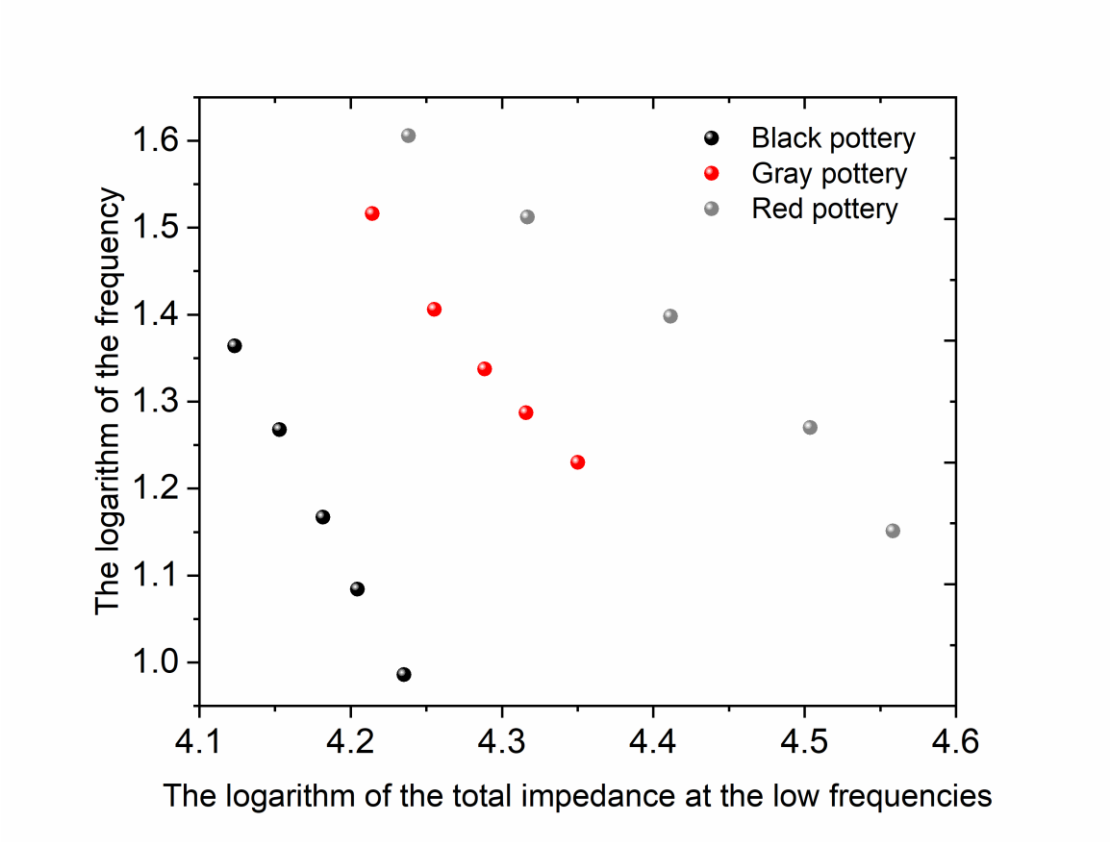

Figure 7. Plots of the logarithm of the total impedance at the low frequencies vs. the logarithm of the frequency for black pottery, gray pottery and red pottery.

4. CONCLUSION

In conclusion, this study confirmed that differential pulse voltammetry and electrochemical impedance spectroscopy can be used as effective tools for pottery analysis. The results indicate that the electrochemical oxidation and reduction of Mn and Fe species could reflect the different materials and/or different production conditions used to make the pottery. The results indicate that electrochemistry could be used for potential archaeological analysis in pottery products.

ACKNOWLEDGEMENTS
This study was supported by Henan Key Laboratory of Research for Central Plains Ancient Ceramics Open Project (ZYGTCXW2018-01).

References

1. E.V. Sayre, R.W. Dodson, D.B. Thompson, *Am. J. Archaeol.*, 61 (1957) 35.
2. M. Tite, *Archaeometry*, 11 (1969) 131.
3. S. Meloni, M. Oddone, N. Genova, A. Cairo, *J. Radioanal. Nucl. Chem.*, 244 (2000) 553.
4. M.S. Tite, *J. Archaeol. Method Theory*, 6 (1999) 181.
5. R.A. Cook, S. Sakai, R.A. Genheimer, *J. Archaeol. Sci. Rep.*, 15 (2017) 132.
6. Ph. Sciau, L. Noé, Ph. Colomban, *Ceram. Int.*, 42 (2016) 15349.
7. A. De Bonis, I. Arienzo, M. D'Antonio, L. Franciosi, C. Germinario, C. Grifa, V. Guarino, A. Langella, V. Morra, *J. Archaeol. Sci.*, 94 (2018) 51.
8. L. Byszewski, A. Tabor, *Surf. Interface Anal.*, 43 (2011) 1108.
9. C. Lofrumento, A. Zoppi, E.M. Castellucci, *J. Raman Spectrosc.*, 35 (2010) 650.
10. C. Rathossi, P. Tsoliskatagas, C. Katagas, *Mineral. Mag.*, 74 (2010) 747.
11. G.A. Cox, A.M. Pollard, *J. Archaeol. Sci.*, 8 (1981) 121.
12. J. Injuk, J. Injuk, *Anal. Chim. Acta*, 300 (1995) 337.
13. A.J. Shortland, K. Domoney, S. Kuhn, *Powder Diffr.*, 25 (2010) 216.
14. R. Sitko, B. Zawisza, J. Jurczyk, D. Bochenek, M. Płoñska, *Microchim. Acta*, 144 (2004) 9.
15. M. Asadi-Eydivand, M. Solati-Hashjin, A. Farzadi, N.A.A. Osman, *Ceram. Int.*, 40 (2014) 12439.
16. A. Farzadi, F. Bakhshi, M. Solati-Hashjin, M. Asadi-Eydivand, N.A.A. Osman, *Ceram. Int.*, 40 (2014) 6021.
17. M. García-Heras, R. Fernández-Ruiz, J.D. Tornero, *J. Archaeol. Sci.*, 24 (1997) 1003.
18. A.T. Rad, M. Solati-Hashjin, N.A.A. Osman, S. Faghihi, *Ceram. Int.*, 40 (2014) 12681.
19. D. Garbeschonberg, S. Muller, *J. Anal. At. Spectrom.*, 29 (2014) 990.
20. B. Hashimoto, H. Daidoji, H. Uchihara, K. Iwasaki, Y. Okamoto, T. Fujiwara, *Anal. Lett.*, 46 (2013) 1299.
21. D. Sakate, Y. Iwazaki, Y. Kon, T. Yokoyama, M. Ohata, *Anal. Sci.*, 34 (2018) 739.
22. L.I. T. K, D.A. Hirschfeld, J.J. Brown, *J. Mater. Sci.*, 32 (1997) 4455.
23. X. Wei, X. Wan, X. Yao, *J. Electroceramics*, 21 (2008) 226
24. E. Iakovleva, E. Mäkilä, J. Salonen, M. Sitarz, M. Sillanpää, *Chem. Eng. J.*, 259 (2015) 364.
25. M.J. Iqbal, ISMAIL, Bushra, *J. Alloys Compd.*, 504 (2010) 440.
26. W.H. Shih, Y.S. Wan, S.I. Kim, I.A. Aksay, *Mrs Proc.*, 289 (1992) 540.
27. V. Tudisca, C. Casieri, F. Demma, M. Diaz, L. Piñol, C. Terenzi, F.D. Luca, *J. Archaeol. Sci.*, 38 (2011) 352.
28. F. Scholz, L. Nitschke, G. Henrion, *Naturwissenschaften*, 76 (1989) 71.
29. F. Scholz, L. Nitschke, G. Henrion, F. Damaschun, *Naturwissenschaften*, 76 (1989) 167.

30. G. Inzelt, *J. Solid State Electrochem.*, 6 (2002) 265.
31. Komorsky-Lovrić, Šebojka; Mirčeski, V. Scholz, Fritz, *Mikrochim. Acta*, 132 (1999) 67.
32. F. Scholz, B. Meyer, *Solid State Ion.*, 23 (1994) 29.
33. F. Scholz, U. Schröder, S. Meyer, K.Z. Brainina, N.F. Zakhachuk, N.V. Sobolev, O.A. Kozmenko, *J. Electroanal. Chem.*, 385 (1995) 139.
34. T. Jamali, H. Karimi-Maleh, M.A. Khalilzadeh, *LWT - Food Sci. Technol.*, 57 (2014) 679.
35. A. Baghizadeh, H. Karimi-Maleh, Z. Khoshnama, A. Hassankhani, M. Abbasghorbani, *Food Anal. Methods*, 8 (2015) 549.
36. H. Karimi-Maleh, F. Karimi, M. Alizadeh, A.L. Sanati, *Chem. Rec.*, (2020) in-press.
37. H. Karimi-Maleh, A.F. Shojaei, K. Tabatabaeian, F. Karimi, S. Shakeri, R. Moradi, *Biosens. Bioelectron.*, 86 (2016) 879.
38. S.A.R. Alavi-Tabari, M.A. Khalilzadeh, H. Karimi-Maleh, *J. Electroanal. Chem.*, 811 (2018) 84.
39. H. Rong, H. Hu, J. Zhang, J. Wang, M. Zhang, G. Qin, Y. Zhang, X. Zhang, *J. Mater. Sci. Technol.*, 35 (2019) 2485.
40. Y. Xu, Y. Lu, P. Zhang, Y. Wang, Y. Zheng, L. Fu, H. Zhang, C.-T. Lin, A. Yu, *Bioelectrochemistry*, 133 (2020) 107455.
41. J. Ying, Y. Zheng, H. Zhang, L. Fu, *Rev. Mex. Ing. Quím.*, 19 (2020) 585.
42. A. Doménech-Carbó, M.T. Doménech-Carbó, M. Moya-Moreno, J.V. Gimeno-Adelantado, F. Bosch-Reig, *Anal. Chim. Acta*, 407 (2000) 275.
43. A. Doménech-Carbó, J.V. Gimeno-Adelantado, F. Bosch-Reig, S. Sánchez-Ramos, M.T. Doménech-Carbó, M.C. Saurí-Peris, *Analyst*, 126 (2001) 1764.
44. A. Doménech-Carbó, M.T. Doménech-Carbó, *Electroanalysis*, 17 (2010) 1959.
45. A. Doménech-Carbó, M.T. Doménech-Carbó, L. Osete-Cortina, J.V. Gimeno-Adelantado, S. Sánchez-Ramos, F. Bosch-Reig, *Electroanalysis*, 15 (2010) 1465.
46. A. Doménech-Carbó, S. Sánchez-Ramosa, M.T. Doménech-Carbó, J.V. Gimeno-Adelantado, F. Bosch-Reig, D.J. Yusá-Marco, M.C. Saurí-Peris, *Electroanalysis*, 14 (2015) 685.
47. D. Mancey, D. Shoesmith, J. Lipkowski, A. McBride, J. Noel, *J. Electrochem. Soc.*, 140 (1993) 637.
48. T. Grygar, *J. Solid State Electrochem.*, 1 (1997) 77.
49. P. Encinas, L. Lorenzo, M. Tascón, M. Vázquez, P. Sánchez-Batanero, *J. Electroanal. Chem.*, 371 (1994) 161.
50. T. Grygar, *J. Solid State Electrochem.*, 2 (1998) 127.
51. T. Grygar, *J. Electroanal. Chem.*, 405 (1996) 117.
52. R. Singh, J. Singh, B. Lal, M. Thomas, S. Bera, *Electrochimica Acta*, 51 (2006) 5515.
53. A. Doménech-Carbó, M. Doménech-Carbó, L. Osete-Cortina, *Electroanal. Int. J. Devoted Fundam. Pract. Asp. Electroanal.*, 13 (2001) 927.
54. L. La-Torre-Riveros, A. Doménech-Carbó, C.R. Cabrera, M.T. Doménech-Carbó, W. Huahuasoncco-Condori, D.Q. Guzmán, M. del Carmen Gutiérrez-Castillo, K. Carmona-Ochoa, A. Pérez-Trujillo, *J. Solid State Electrochem.*, 23 (2019) 1541.